Supporting Information for "Stratigraphic reconstruction and analysis of the delta remnant Kodiak in Jezero Crater, Mars"

C. D. Tate[1], A. H. Hayes[1], O. A. Kanine[2], S. Gupta[3], G. Caravaca[4], G. Paar[5], S. Le Mouélic[6], C. Traxler[7], J. Rice[8]

[1]Cornell University, Department of Astronomy and Planetary Science, Ithaca, NY, USA
[2]California Institute of Technology Division of Geological and Planetary Sciences, Pasadena, CA, USA
[3]Imperial College London, Department of Earth Science and Engineering, London, UK
[4]Institut de Recherche en Astrophysique et Planétologie, CNRS, Université de Toulouse, CNES, France
[5]Joanneum Research, Institute for Digital Technology, Graz, Austria
[6]CNRS Délégation Bretagne et Pays de Loire, Nantes, France
[7]VRVis Zentrum für Virtual Reality und Visualisierung Forschungs-GmbH, Wien, Austria
[8]Arizona State University, School of Earth and Space Exploration, Tempe, AZ, USA

Contents of this file

1. Text S1 to S5
2. Tables S1 and S2
3. Figure S1 to S4

Additional Supporting Information (Files uploaded separately)

1. OBJ wavefront model of Kodiak
2. PNG orthographic images of Kodiak described in S3
3. Excel spreadsheet, "tables.xlsx" with Tables 1, 2, S1, S2, and other information described in S4
4. PRo3D Annotation file described in S4

S1. Mars 2020 observations

Tables S1 and S2 list the Mars 2020 observations of Kodiak for the first 800 sols of the Mars 2020 mission. The Mastcam-Z observations (Table S1) are limited to images taken at its highest resolution zoom level at 110 mm. The Sol is the Martian day after landing, and the LMST is the local mean standard time. The sequence identification numbers are given for each. The azimuth and range values are measured from the rover's imaging location to the northeast edge of Kodiak. The resolution (Res.) is the pixel scale at Kodiak's distance (the product of the distance and Mastcam-Z 110mm ifov). The "used" column denotes whether the images were included in Kodiak's final reconstruction. The primary reason for not using a set of images is because they were taken at times of day with unfavorable lighting. Sols 418 and 548 imaged Kodiak when it was backlit and largely shadowed. This was more of an issue for the SuperCam RMI images since this solar geometry caused high levels of stray light in its optics and rendered the images unusable. Note that S1 does not include images taken at focal lengths other than 110mm. Our reconstruction used several 34 mm and 63 mm mosaics of Kodiak when their locations filled large gaps in the 110 mm dataset or helped make the control point network more robust. We similarly used Navcam images for the early stages of aligning widely spaced image stations.

S2. Reconstruction Range Error

0094-8276/23/$5.00

Equation 1 gives the pixel scale s of an image taken from a distance d from its target. Pixel scale estimates the best possible resolution the camera can achieve without super-resolution. A camera's actual resolution, or the limit of its resolving power, is typically much larger than one pixel.

$$s = id. \tag{1}$$

Equation 2 gives the precision with which a pair of stereo images can estimate the range of a feature correspondent in both images. This equation comes from the Mars 2020 Camera Software Interface Specification (SIS) (?, ?), which describes the PDS-compliant image data products from all Mars 2020 cameras.

$$e = ic\frac{r^2}{b}, \tag{2}$$

where e is the range error, i is the camera's instantaneous field of view ($ifov = 67\ \mu rad$ for Mastcam-Z at 110mm focal length), c is the correlation accuracy in pixels (usually $c = 0.25$ pixels), r is the stereo range distance, and b is the effective baseline between the two imaging locations. This range error estimation is appropriate for stereo pairs taken under identical lighting conditions and at small angular separations, $b/r \ll 1$. Although this equation simplifies a complex problem, it must be enfranchised that eq 2 breaks down for large baseline distances relative to range. For instance, the maximum stereo disparity in this dataset is between azimuths, $az_{max} - az_{min} = 140°$, for which $b > r$ and eq. 2 would not give an appropriate estimate range error. Therefore, it is necessary to account for what happens to reconstruction errors for an arbitrary number of stereo pairs with pair-wise stereo disparities that do not follow the small angle approximation.

Estimating realistic range errors requires accounting for several second-order effects absent in eq. 2. Foremost, structure from motion (SfM) is a multi-stereo technique not strictly limited by individual stereo pairs (refs). Another effect not captured in eq. 2 is how the stereo correlation parameter c changes with increasing stereo disparity ratio b/r. Undoubtedly, the correlation becomes less precise as the projected features on the terrain surface diverge at wide angles. Part of this effect would be due to the breakdown in the small angle approximation. Still, the primary cause would be the inherent confusion in the tie point matching between the stereo pairs over terrain with complex topography. Although this becomes a scene-relevant source of error,

we wish to identify a reasonable limit on the stereo disparity ratio. One such limit happens at a disparity angle of 14 degrees (or a disparity ratio of $b/r = 0.25$), beyond which eq. 2 could significantly underestimate the range error. Taking a maximum stereo disparity ratio of $(b/r)_{max} \approx 0.25 \approx c$, the minimum range error becomes the product of ifov and range, which simplifies to the approximate pixel scale,

$$e_{min} = ir. \tag{3}$$

Notably, this minimum range error approximately equals the pixel scale $e_{min}(r) \approx s(d)$ where $r \approx d$. Since it does not make physical sense for range error to be more precise than the lateral pixel scale, $e < s$, we justify $(b/r)_{max} \approx c$ as a reasonable limit on the meaningful extracting of topological information from stereo imaging. Therefore, we estimate the range error by evaluating eq. 2 at average adjacent disparity angles of the dataset taken from $N = 20$ imaging locations,

$$(b/r)_{eff} = tan\left(\frac{az_{max} - az_{min}}{N-1}\right) \approx 0.13, \tag{4}$$

which is 7° disparity angle. The effective disparity ratio can also be assumed to be half of the maximum value, $(b/r)_{eff} \approx \frac{1}{2}(b/r)_{max} \approx \frac{1}{2}c$. In either case, the effective maximum range error of this dataset is approximately twice the pixel scale,

$$e_{max} \approx 2id. \tag{5}$$

In the present case for a model made from a large number of imaging locations ($N \gg 2$) that are semi-uniformly distributed over an extensive range of azimuths ($az_{max} - az_{min} \gg 1$), the estimated range error is reasonably between the pixel scale and twice the pixel scale, $s < e \leq 2s$. For simplicity, therefore, we can assume that the range error of this SfM reconstruction is equivalent to the pixel scale.

S3. Orthographic maps and projections of Kodiak

The images in Fig. 3 are orthographic renderings of the model from four directions: up, north, east, and northeast. We uploaded full-resolution PNG images separately in the supplemental data. We include several other orthographic projections. These include a set of three images that show Kodiak's northern outcrops from approximately the Sol 580 location with the Mastcam-Z images (Fig. S4b), SuperCam images (Fig. S4c), and both (Fig. S4d) projected onto our model of Kodiak.

S4. PRo3D

We use PRo3D for our 3D analysis. Fig. S2 shows a sample of the layer traces used in this study. We present a complete record of our traces in several forms. The attached spreadsheet ("tables.xlsx") has a tab named "Table A3" that gives high-level information about each of the two dozen regions on Kodiak where we performed quantitative strike and dip analysis. This table shows the region name (arbitrarily assigned), type (e.g., topset, foreset, bottomset), medium dip angle, medium dip azimuth, number of measurements, and a PRo3D screenshot graphically showing its location on Kodiak. Another tab, "Table A3 long version" gives the measurement and uncertainty values for every line trace. This includes each measurement strike (azimuth minus 90 degrees), dip angle, rake angle, and the max and min angular error estimated by the PCA-based plane-fitting algorithm (Quinn & Ehlmann (2019)). Additional columns give the trace's region name as defined in tab "Table A3"; the dip color using the same color map as Fig. 3 (a); and the number of points we selected on the model to define the trace. We ordered the first six columns of tab "Table A3 long version" for direct copy and paste into Daven Quinn's website, Uncertain orientations plotter `https://davenquinn.com/projects/attitude/plotter`. This tool specializes in graphically inspecting the error space of strike and dip measurements.

S5. Additional measurements on Kodiak and Whale Mountain

Whale Mt. is attached to the Western Jezero Delta and stands about 1 km west of Kodiak. There are several notable similarities and differences between these two geological features. It could be a coincidence that Whale Mt is the closest part of the delta to Kodiak. Figure S3 is similar to Figure 3 but lacks several annotations that may obscure some features of interest. Figure S4 shows our dip and strike measurements on Whale Mountain, which preserves a delta lobe-like feature similar in scale to the northeast "nose" of Kodiak.

The primary similarity is Whale Mt's dome-shaped layers to the nose of Kodiak's Unit 1. The layers in Whale Mt dip between azimuths of 60 and 210 with a median value of about 120 N. This direction is nearly orthogonal to Kodiak's nose, which dips between 180 to 240 N with a median of about 200 N. Both features have consistently changing layers over scales of 50 m. This scale is small for a Gilbert-style delta foreset. However, this is less likely to be an anomaly because there are two examples in the delta front area.

Table S1. Mastcam-Z observations of Kodiak taken at its highest zoom lever at 110mm focal length. The images taken after Sol 580 are not used our 3D reconstruction.

Sol	LMST	Sequence	Azimuth [°N]	Range [m]	Res. [cm/pix]	Used	Notes
4	14:07	zcam00024	84.0	2298	16	no	-
57	10:48	zcam08103	84.0	2369	17	yes	-
63	8:29	zcam08022	84.0	2369	17	no	with Scam RMI
69	8:46	zcam03120	84.4	2376	17	no	-
77	7:32	zcam08036	85.0	2390	17	no	with Scam RMI
83	7:58	zcam03132	85.0	2390	17	yes	Scam RMI
94	12:14	zcam08054	85.3	2368	17	no	too late in day
104	12:30	zcam08065	86.4	2307	16	no	too late in day
105	15:26	zcam08071	87.8	2276	16	no	too late in day
108	11:46	zcam08075	88.0	2275	16	yes	only south side visible
111	10:43	zcam08084	90.5	2215	16	yes	-
114	12:08	zcam08092	91.4	2210	15	no	too late in day
121	11:38	zcam08114	92.2	2203	15	no	-
128	10:45	zcam08128	94.7	2240	16	yes	-
130	11:30	zcam08132	95.1	2267	16	no	-
135	10:46	zcam08138	101.2	2411	17	yes	-
149	11:49	zcam08160	104.6	2436	17	no	occluded
207	12:35	zcam08235	102.8	1856	13	no	occluded
214	10:54	zcam08251	102.2	1835	13	yes	occluded
248	8:27	zcam08270	101.6	1882	13	no	with Scam RMI
275	9:17	zcam08292	101.6	1882	13	yes	-
284	11:45	zcam08305	102.8	1837	13	no	Kodiak occluded
290	7:32	zcam08315	104.5	1809	13	no	Kodiak occluded
382	9:36	zcam08410	78.8	2528	18	yes	-
383	9:36	zcam08411	77.2	2809	20	yes	-
388	8:10	zcam08416	64.2	3212	22	yes	very long distance
409	10:10	zcam08425	18.8	784	5	yes	-
414	10:04	zcam08428	-3.4	701	5	yes	-
415	15:40	zcam08430	-24.0	527	4	yes	-
416	16:00	zcam08433	-28.9	478	3	yes	-
418	10:09	zcam08438	-28.9	478	3	no	with Scam RMI
470	12:49	zcam08491	-9.8	1050	7	yes	too late in day
548	13:00	zcam08565	-23.3	580	4	no	with Scam RMI, stray light
580	15:11	zcam08598	-36.3	701	5	yes	with Scam RMI
693	12:35	zcam08688	-3.8	717	5	no	after sol 580
711	11:28	zcam08714	-16.1	1255	9	no	after sol 580
753	16:03	zcam08758	-43.6	2397	17	no	after sol 580
756	15:43	zcam08765	-44.5	2514	18	no	after sol 580
762	11:46	zcam08774	-40.1	2521	18	no	after sol 580

Table S2. SupterCam RMI imaging sequences of Kodiak.

Sol	LMST	Sequence	Azimuth [°N]	Range [m]	Res. [cm/pix]	Images	Used	Notes
63	8:12	scam01063	84.0	2369	2.47	10	yes	-
77	8:25	scam02077	85.0	2390	2.50	2	yes	-
248	8:06	scam01248	101.6	1882	1.97	10	yes	-
418	8:57	scam01418	-28.9	478	0.50	10	no	stray light
548	12:40	scam04548	-23.3	580	0.61	4	no	stray light
548	12:50	scam05548	-23.3	580	0.61	4	no	stray light
580	15:17	scam01580	-36.3	701	0.73	12	yes	-

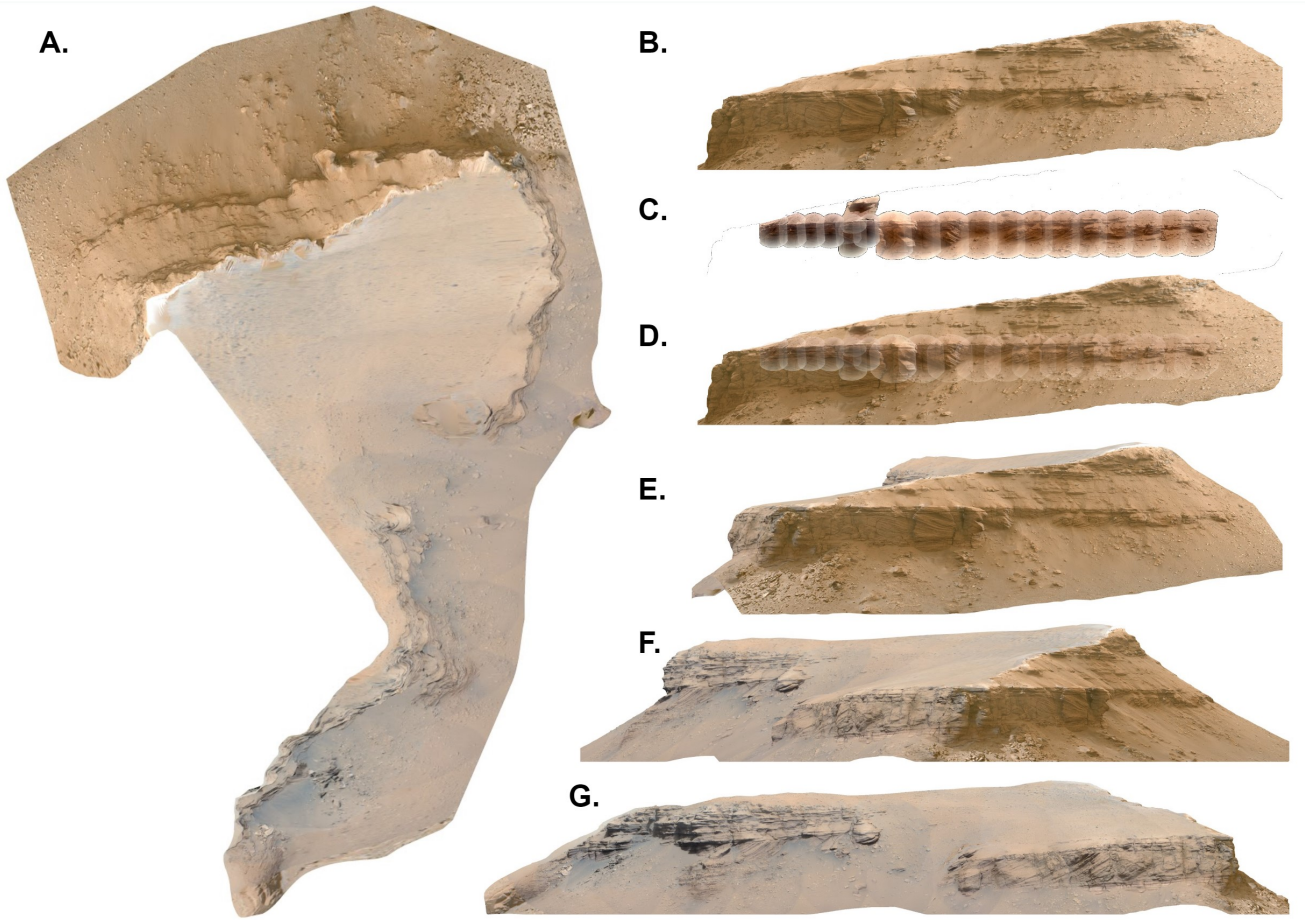

Figure S1. Rendered Orthographic Images of Kodiak. The full-scale images are downloadable from supplementary materials. Each image filename is in parentheses below. (a) plane view same as Fig. 3a (Kodiak_top.png); (b) Kodiak's northern outcrops from approximately the Sol 580 location (Kodiak_sol580_scam_only.png); (c) is the same as (b) but with only SuperCam RMI image projections (Kodiak_sol580_scam_only.png); (d) is the same as (b) and (c) with the Supercam RMI images projected on top of the Mastcam-Z images (Kodiak_sol580_scam_zcam.png); (e) northern view and same as Fig. 3b (Kodiak_north.png); (f) northeastern view and same as Fig. 3c (Kodiak_northeast.png); (g) eastern view and same as Fig. 3d (Kodiak_east.png)

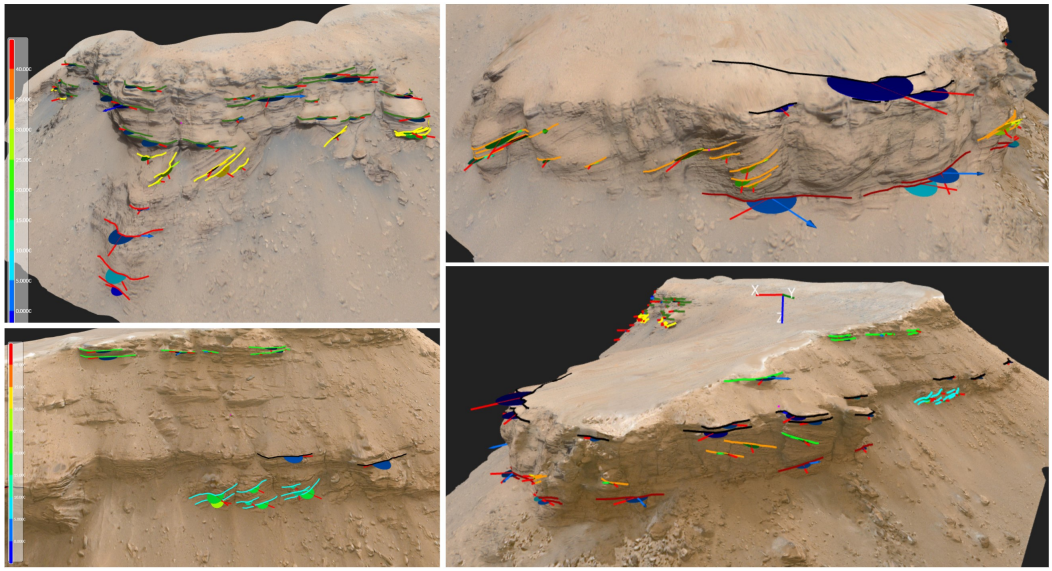

Figure S2. Views from the PRo3D software, in which we trace the best-exposed layers and solve for their geometric properties.

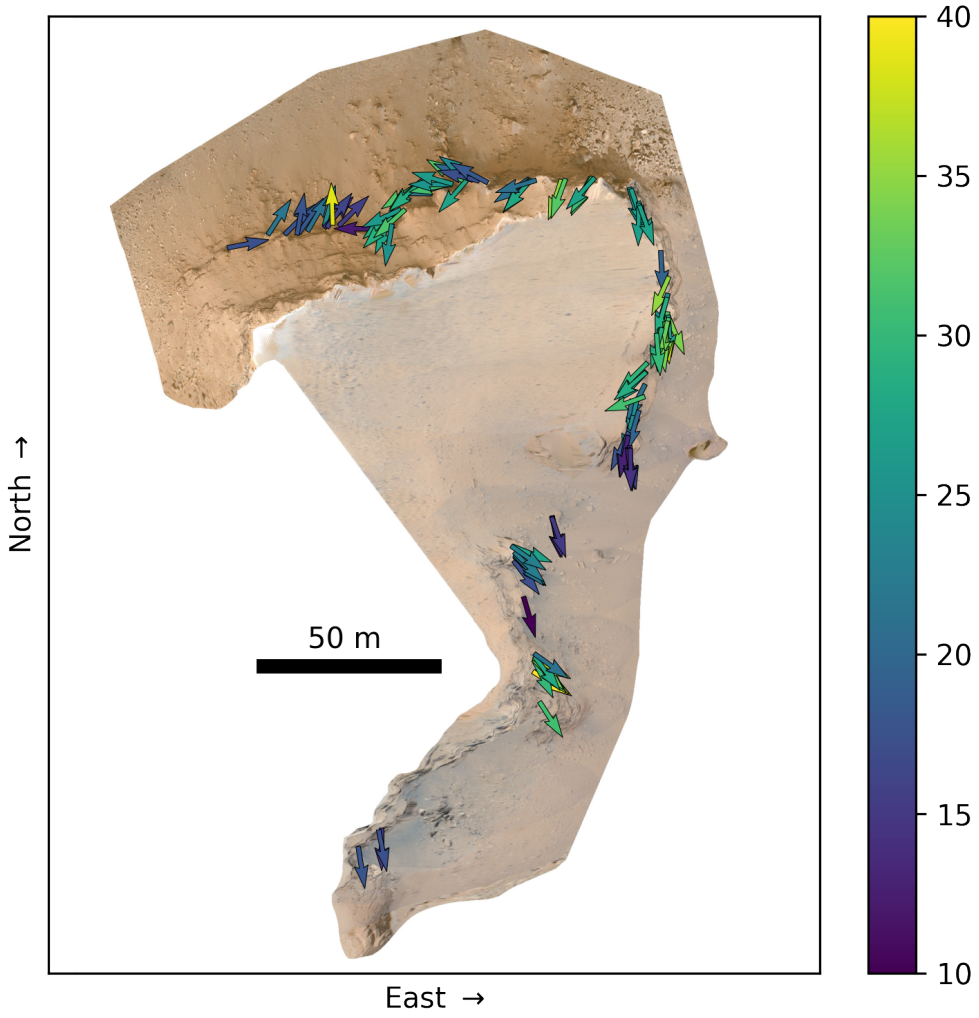

Figure S3. Orthgraphic projection Kodiak with strike and dip annotations. These data are identical to Fig. 3.

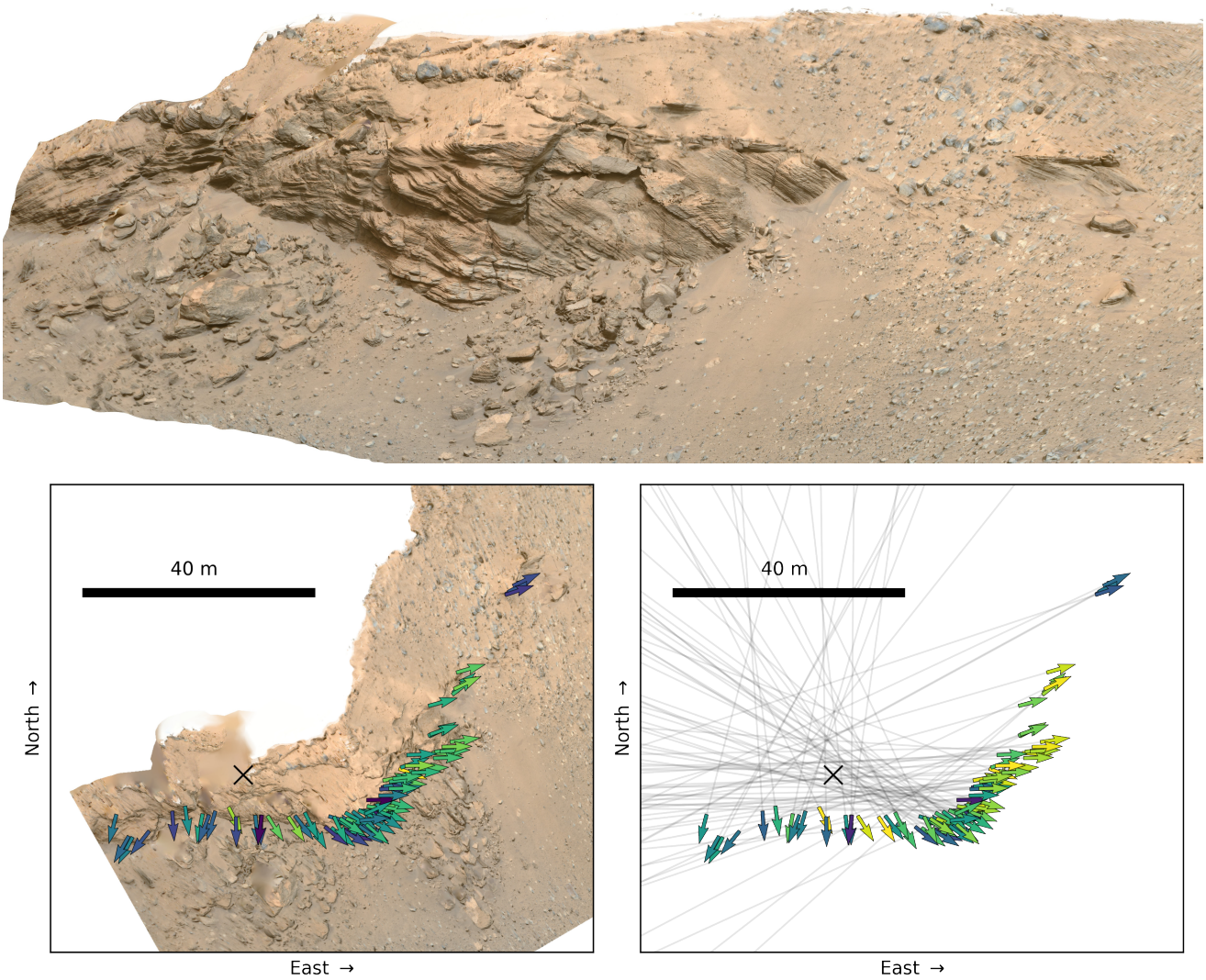

Figure S4. Orthgraphic projections of Whale Mountain and strike and dip annotations. The top image (a) is Whale Mountain from the Northeast direction. In this projection, up is up, and right is Northwest [add subplot letters, a North arrow, and a scalebar]. The bottom left (b) is a plane view orthographic projection with arrows showing the dip azimuths and color showing the dip angle. The bottom right (c) shows lines extending from. The dip colors use the same colorbar scale as Fig. S4.